IMPLICIT LARGE EDDY SIMULATION OF A SUPERSONIC TURBULENT BOUNDARY LAYER OVER A COMPRESSION-EXPANSION RAMP

Muzio Grilli[1], **Stefan Hickel**[1] **and Nikolaus A. Adams**[1]
[1]Lehrstuhl für Aerodynamik und Strömungsmechanik
Technische Universität München
Boltzmannstr 15, D-85748 Garching, Germany
muzio.grilli@aer.mw.tum.de

ABSTRACT

Results of a large-eddy simulation (LES) of a supersonic turbulent boundary layer flow along a compression-expansion ramp configuration are presented. The numerical simulation is directly compared with an available experiment at the same flow conditions. The compression-expansion ramp has a deflection angle of $\beta = 25^\circ$. The flow is characterized by a free-stream Mach number of $Ma_\infty = 2.88$ and the Reynolds number based on the incoming boundary layer thickness is $Re_{\delta_0} = 132840$. The Navier Stokes equations for compressible flows are solved on a cartesian collocated grid. About 32.5×10^6 grid points are used to discretize the computational domain. Subgrid scale effects are modeled implicitly by the adaptive local deconvolution method (ALDM). A synthetic inflow-turbulence technique is used, which does not introduce any low frequency into the domain, therefore avoiding any possible interference with the shock/boundary layer interaction system. Statistical samples are gathered over 1000 characteristic time scales δ_0/U_∞. The numerical data is in good agreement with the experiment in terms of mean surface-pressure distribution, skin-friction, mean velocity profiles, velocity and density fluctuations. The computational results confirm theoretical and experimental results on fluctuation-amplification across the interaction region. In the wake of the main shock a shedding of shocklets is observed. Results show the development of Görtler-like vortices in the reattachment region. The LES provide a reliable and detailed flow information, which helped to improve considerably the understanding of shock-boundary-layer interaction.

1 INTRODUCTION

The design process of supersonic and hypersonic air vehicles requires accurate simulation methods in order to predict aero-thermodynamic loads. The need to achieve an optimal and safe design poses the requirement of an accurate estimation of critical quantities such as skin friction, heat-transfer rates, mean and fluctuating pressure. The interaction of turbulent boundary layers with shocks and rarefaction waves is one of the most prevalent phenomena occurring in high-speed flight, which can affect significantly the aero-thermodynamic loads. Accurate computations of such interaction are needed to gain a deeper insight into many aspects of this phenomenon which is still not fully understood, including the dynamics of shock unsteadiness, turbulence amplification through the shock, unsteady heat transfer near the separation and reattachment points and turbulence damping by the interaction with a Prandtl-Meyer expansion.

Numerous Direct Numerical Simulations (DNS) and LES computations were carried out in the past for the compression ramp configuration (Adams (2000), Loginov et al. (2006), Wu & Martin (2007)) but the whole compression-expansion ramp configuration was never taken into account for a detailed simulation. In the present work we compare our results with the experimental data from Zheltovodov et al. (1990). The experiments were performed using two models having the same shape but different linear scales. The larger model was used for a detailed investigation of the mean flow with a free-stream Mach number of $Ma_\infty = 2.88$ and a Reynolds number based on the incoming boundary layer thickness of $Re_{\delta_0} = 132840$. The turbulence characteristics are investigated using the small model with a free-stream Mach number of $Ma_\infty = 2.95$ and $Re_{\delta_0} = 63560$. The experimentally obtained flow field and the measurement stations are sketched in Fig. 1 for both mentioned configurations of the 25^o compression-expansion ramp. In the present work the conditions of the large model are chosen, but a comparison is also carried out with the turbulence data obtained from the small model by scaling them with the local boundary layer thickness. The present work aims to assess the prediction quality of the employed numerical techinque by matching directly the experimental parameters. Given the successful validation, the computational results provide a reliable database for further analysis.

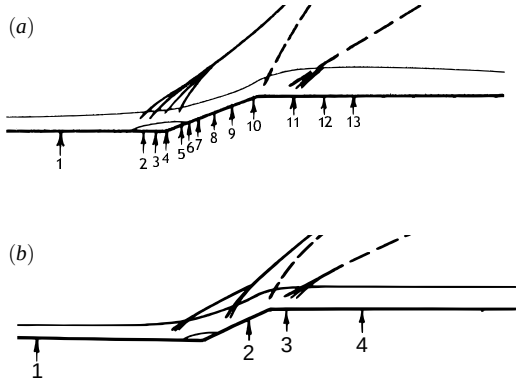

Figure 1. Experimenatal measurement sections for the large (a) and small (b) model.

Table 1. Streamwise locatoin of the measurement stations.

Large Model		Small Model	
Station	x/δ_0	Station	x/δ_0
E1	-8.05	T1	-15.42
E2	-2.93	T2	4.41
E3	-1.95	T3	7.93
E4	-1.22	T4	14.98
E5	1.22		
E6	2.68		
E7	3.05		
E8	4.15		
E9	5.73		
E10	7.56		
E11	12.20		
E12	15.24		
E13	19.15		

2 FLOW CONFIGURATION

The computational domain, shown in Fig. 2, has the extents $L_x = 41.25\ \delta_0$, $L_y = 12\ \delta_0$ and $L_z = 4\ \delta_0$. The spanwise domain size is chosen wide enough so that large-scale coherent structures such as Görtler-like vortices can be captured. The computational grid, shown in Fig. 3, has been generated with an adaptive mesh refinement procedure which guarantees that the first point in the wall-normal direction at the inlet, with respect to the ramp geometry, is located at $y^+ \approx 2.2$. Such resolution was found to be enough to reproduce the experimental results in the first reference section E1 with sufficient accuracy. The grid spacing in the streamwise direction is $\Delta x^+ \approx 52.9$ and in the spanwise direction a resolution of $\Delta z^+ \approx 25.7$ is adopted.

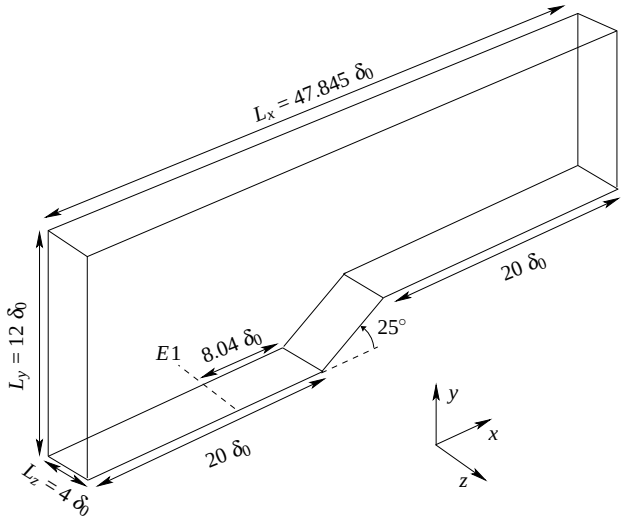

Figure 2. Computational domain of the present LES.

The reference length throughout this work is the mean boundary-layer thickness of the experiment, $\delta_0 = 4.1\ mm$, at the first reference section $E1$. The boundary-layer thickness is measured as the distance from the wall where 99% of the mean free-stream velocity of $U_\infty = 618.1\ m/s$ is reached. Here and in the following, dimensional quantities are indicated by an asterisk. The non-dimensionalization is as follows:

$$\begin{aligned} u_i &= u_i^*/U_\infty^*,\ \rho = \rho^*/\rho_\infty^*,\ T = T^*/T_\infty^*, \\ p &= p^*/(\rho_\infty^* U_\infty^{*2}),\ E = E^*/(\rho_\infty^* U_\infty^{*2})\ . \end{aligned} \tag{1}$$

Reference data are taken from the experiment as $\rho_\infty^* = 0.368\ kg/m^3$ and $T_\infty^* = 114.8\ K$.

The positions of the considered experimental stations in terms of the dimensionless downstream coordinate x/δ_0, measured along the wall from the compression corner position, are summarized in Tab. 1.

3 NUMERICAL APPROACH

The three-dimensional compressible Navier-Stokes equations in conservative form are considered

$$\partial_t \mathbf{U} + \nabla \cdot \mathbf{F}(\mathbf{U}) + \nabla \cdot \mathbf{D}(\mathbf{U}) = \mathbf{0}. \tag{2}$$

The equations are solved in a dimensionless form and with the assumption of an ideal gas. A power law is assumed for the temperature dependence of viscosity and of the thermal conductivity.

The aforementioned governing equations are solved using the Adaptive Local Deconvolution scheme (Hickel & Larsson (2008)) for the discretization of the convective fluxes. A 2^{nd} order central difference scheme is used to compute the

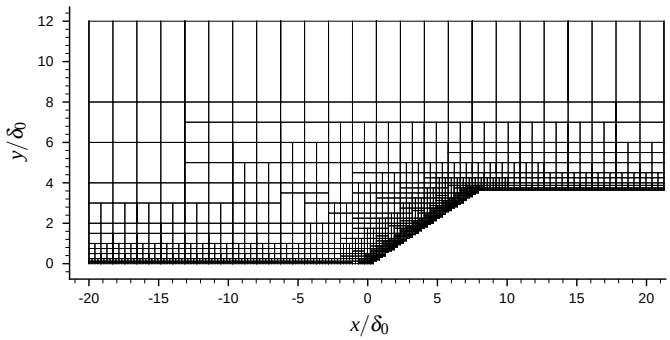

Figure 3. Computational grid of the present LES (each 10^{th} line is shown).

diffusive fluxes and a 3^{rd} order Runge Kutta scheme to integrate in time. Periodic boundary conditions are used in the spanwise direction, whereas an immersed interface method is used to describe the compression ramp geometry, which reproduces an adiabatic no-slip wall. The top (freestream) and outflow boundaries make use of a linear extrapolation procedure. A synthetic turbulence inflow technique (Touber & Sandham (2009)) is used, which is designed to match ad hoc first- and second-order statistical moments and spectra. The adoption of such a technique avoids the introduction of any low frequency into the domain, therefore avoiding any possible interference with the shock/boundary layer interaction system.

4 COMPRESSION-EXPANSION RAMP FLOW

An instantaneous snapshot of the computed Schlieren-type visualization (Fig. 3a) reveals similarities with experimental picture (Fig. 3b). The undisturbed boundary layer (1) is affected by the separation shock (2). The interaction results in the appearance of a reverse flow region (3) and of a separated shear layer (4) with traveling shocklets (5) above it. The collapse of this shocklets leads to the generation of the unsteady second stem (6) of the λ-shock configuration. The shocklets cannot be anymore identified as organized structures downstream of the expansion.

4.1 Mean Flow

The wall pressure, normalized by its mean value at the station $E1$, constantly increases during shockwave/boundary layer interaction with a plateau inside the separation zone. It drops later to the initial values in the expansion fan (Fig. 5a). A slight pressure increase in the region $8 < x/\delta_0 < 9$ may indicate the existence of a weak compression wave inside the boundary layer downstream of the expansion.

The mean skin-friction exhibits the typical behavior for a separated flow (Fig. 5b). The initial decrease, at $x/\delta_0 = -20$ is due to the synthetic turbulence technique adopted for the generation of the inflow data. A transient of about $5\delta_0$ is needed for the flow to recover the modeling errors introduced by the digital filter procedure. A slight decrease along the flat plate is then visible since the incoming boundary layer grows and the local Reynolds number increases $(x/\delta_0 < -6)$.

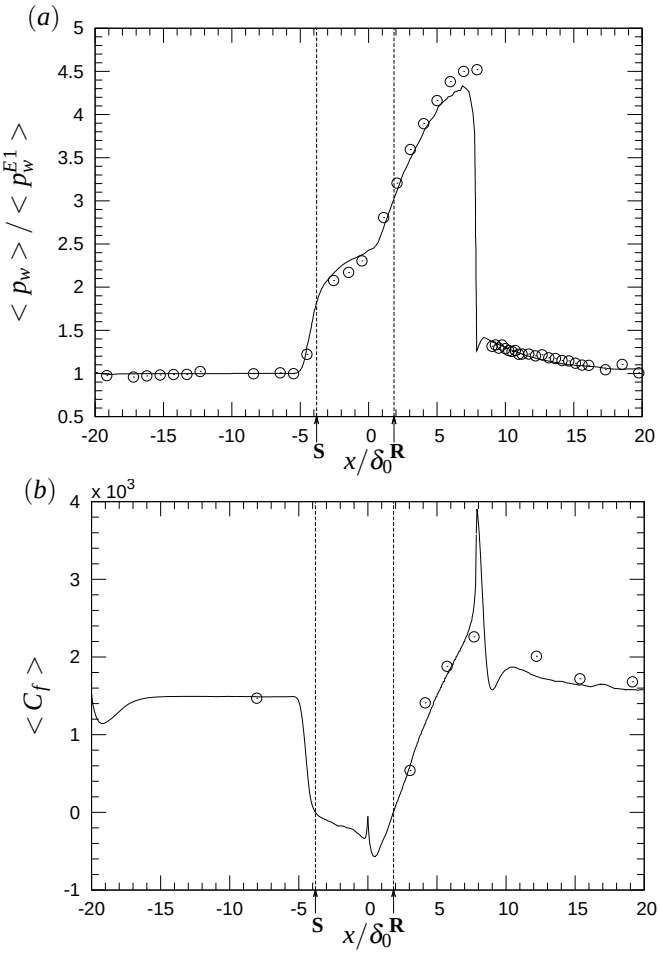

Figure 5. Averaged skin-friction coefficient (a) and wall-pressure (b) distributions in the streamwise direction. ∘ , reference experiment; —— current LES averaged in time and over the spanwise direction. Symbols **S** and **R** indicate the mean separation and reattachment points.

The friction coefficient drops, then, suddenly near the separation point (S) acquiring negative values inside the reverse flow region $(-4.5 < x/\delta_0 < 2.0)$. It rises again after the reattachment point (R) reaching values which are slightly above the incoming ones on the upper surface. The spikes near the compression and the decompression corners are likely due to limited resolution of the corner singularity. Sharp gradients of flow variables occur over a short distance near such locations causing a Gibbs-like oscillation in the numerical solution.

Fig. 6 gives a description of the mean flow evolution in terms of mean streamwise velocity component. The undisturbed incoming turbulent boundary-layer profile in section $E1$ evolves into a profile with weak reverse flow slightly downstream of the separation point (section $E2$). Further downstream the reverse flow becomes stronger (sections $E3-E5$). At section $E6$ the boundary layer attaches again while still showing a momentum deficit in the wake. This re-established attached boundary layer develops towards an undisturbed profile further downstream (sections $E7-E10$). After the expansion fan the boundary layer recovers similar features to the undisturbed incoming condition (sections

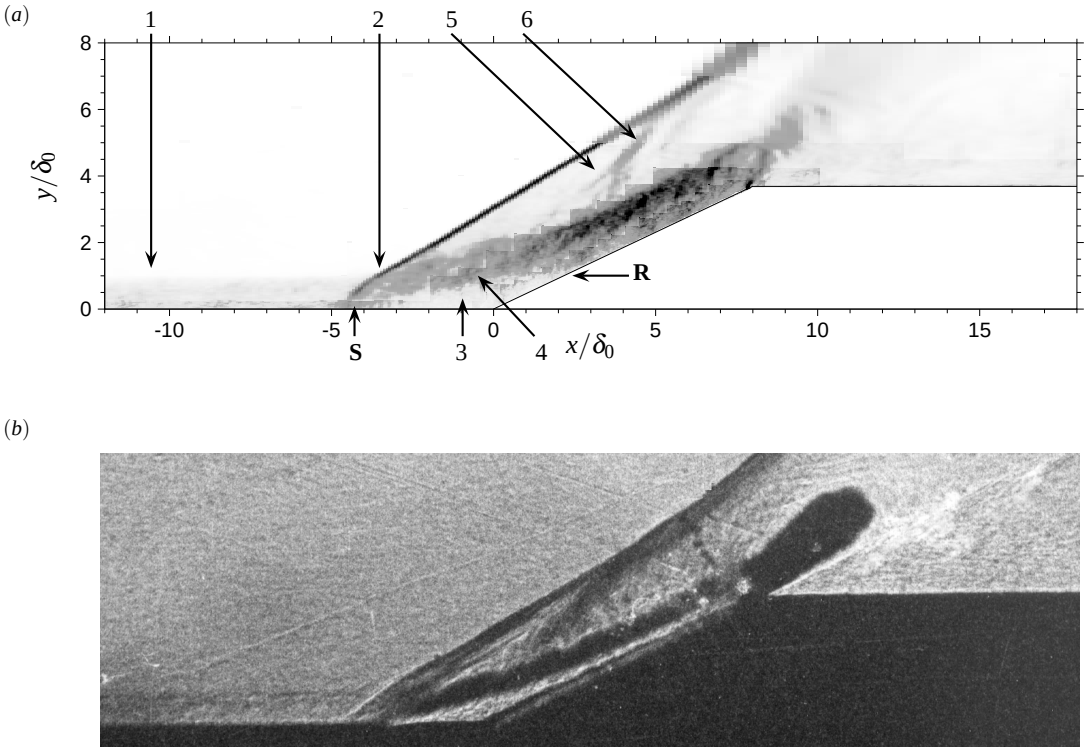

Figure 4. Instantaneous representation of the flow by the Schlieren-type visualization. The computed density gradient averaged in spanwise direction $||\nabla\rho||$ (a) and experimental Schlieren visualization (b).

$E11-E13$). Generally, a good agreement is found between numerical and experimental data. Excessive negative experimental velocities at section $E5$ can be explained by difficulties in measuring the reverse flow.

Root-mean-square (RMS) values of velocity $\sqrt{<u'u'>}$ and density $\sqrt{<\rho'\rho'>}$ fluctuations are shown at the downstream stations $T1-T4$ in Fig. 7. This data refers to the lower Reynolds number experiment carried out on the small model, as mentioned in Sec.1. The location of the measurement sections $T1-T4$ is shown in Tab. 1. The profiles are normalized with the maximum value of the undisturbed boundary layer in accordance with the experiment of Zheltovodov et al. (1990). Since the first section T1 is located outside of the computational domain, its values are compared with turbulence data extracted in the section E1. In agreement with the experiment the RMS values increase after the interaction with the shock (section $T2$) shifting the maximum from a near wall position to the shear layer. The Prandtl-Meyer expansion moves the maximum further away from the wall and damps the RMS values. Fluctuations are rather large outside of the boundary layer. As visible from Fig 7, the RMS profiles at the station $T4$ have different features than the equilibrium boundary layer on the flat plate (station $T1$), consisting in a higher level of turbulence in the outer flow ($y/\delta_0 > 2.5$). The agreement with the experimental data is generally good even if some discrepancies are evident and mainly due to the different Reynolds number of the adopted reference experiment.

Despite the flow geometry being two-dimensional, the interaction between the boundary layer and the shock breaks down the spanwise spanwise homogenity. As already shown in the previous work of Loginov et al. (2006) two pairs of counter-rotating streamwise vortices can be identified in the reattaching shear layer. Such vortices, generally named Görtler vortices, are caused by the streamline curvature.

The spanwise inhomogeneity of the mean C_f, caused by Görtler-like vortices is shown in Fig. 8. The amplitude of the the variation increases from $\pm 0.06\times 10^3$ in the undisturbed boundary layer at the station $E1$ to $\pm 0.3\times 10^3$ in the section $E6$ just after the reattachment. After the decompression corner the amplitude of the variation becomes less pronounced decreasing from $\pm 0.3\times 10^3$ to $\pm 0.1\times 10^3$ at station $E11$. The distribution becomes more uniform without extrema suggesting that the streamwise vortices decay while passing through the expansion fan. Further downstream at station $E13$ the variation reduces almost to the undisturbed value $\pm 0.08\times 10^3$.

Further evidence of the presence of the Görtler vortices is given in Fig. 9, which shows a snapshot of the streamwise velocity fluctuation field in a plane parallel to the compression-expansion ramp wall at $y^+\approx 12$. The colourmap is set in order to higlight the region of the flow with a velocity deficit. On the left side of the domain we can see the typical streaky structure of a turbulent boundary layer. Such structure is then destroyed by the interaction with the shock. After the boundary layer reattachment location a pattern which could be related to two streamwise evolving structures is clearly visible. Such structures could be the signature of the Görtler vortices. This pattern disappears after the passage through the decompression corner and the typical streaky structure of the incoming undisturbed boundary layer is then recovered.

Fig. 10 shows the comparison between a surface oil-flow visualization obtained in the experiments of Zheltovodov & Yakovlev (1986) and the surface skin friction pattern derived

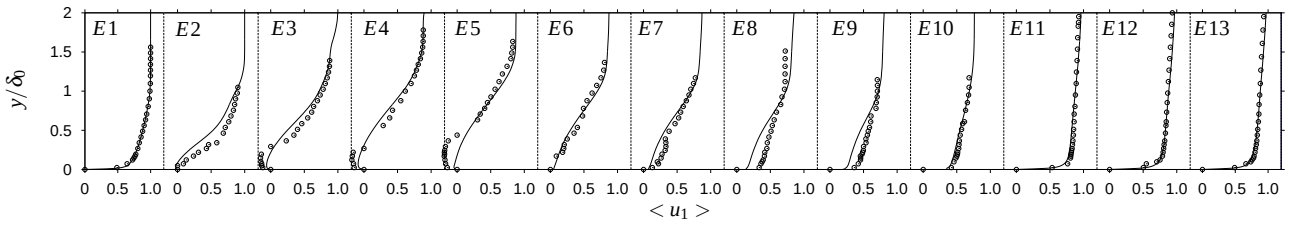

Figure 6. Velocity profiles at stations E1-E13. ○ , reference experiment; —— , current LES averaged in time and over the spanwise direction.

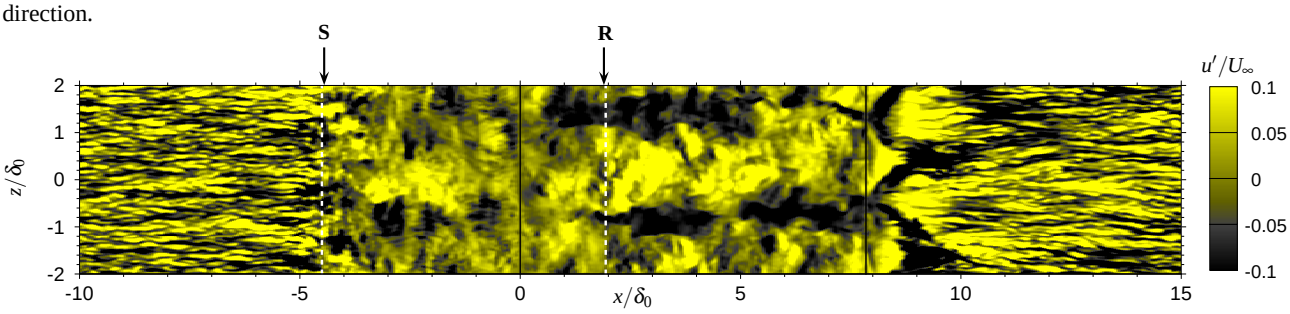

Figure 9. Instantaneous snapshot of u'/U_∞ at $y^+ \approx 12$. Symbols **S** and **R** indicate the mean separation and reattachment points.

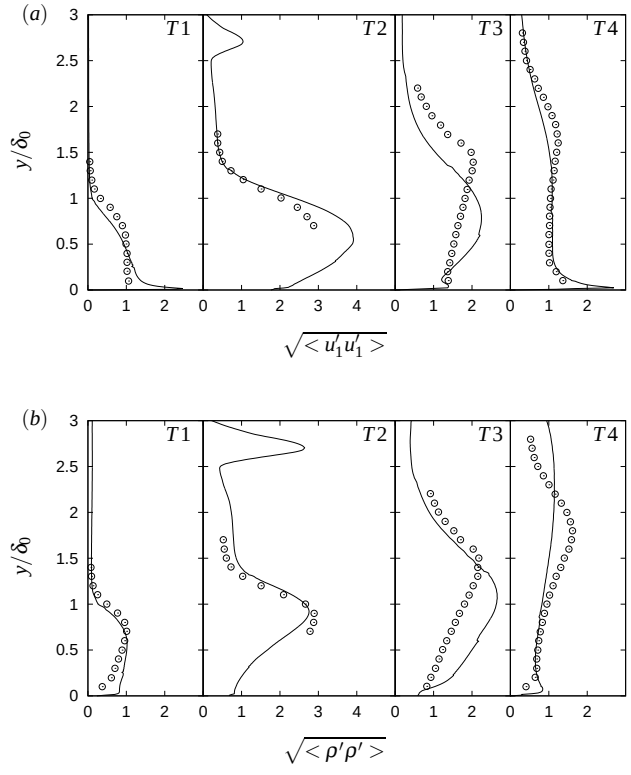

Figure 7. Root-mean-square profiles of the velocity (a) and density (b) fluctuations at stations T1-T4. ○ , reference experiment; —— , current LES averaged in time and over spanwise direction

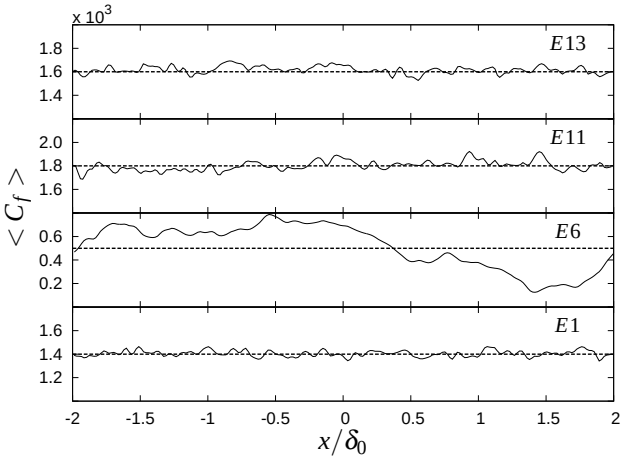

Figure 8. Distribution of the mean skin-friction coefficient at the wall in the spanwise direction. —— , averaged in time; – – – , averaged in time and over spanwise direction.

from the computation. In both the numerical and experimental figures convergence and divergence lines in the reattaching flow are clearly visible. In the computation the pair of convergence and divergence lines is spaced by approximately $2\delta_0$. It should be noted that the computational domain size in the spanwise direction is $4\delta_0$, with periodic boundary conditions applied, allowing for flow structures with spanwise periodicity of at most $4\delta_0$ to be captured.

5 CONCLUSIONS

The numerical investigation of compression-decompression ramp flow was performed using large-eddy simulation. Unprecedentedly, a high Reynolds number

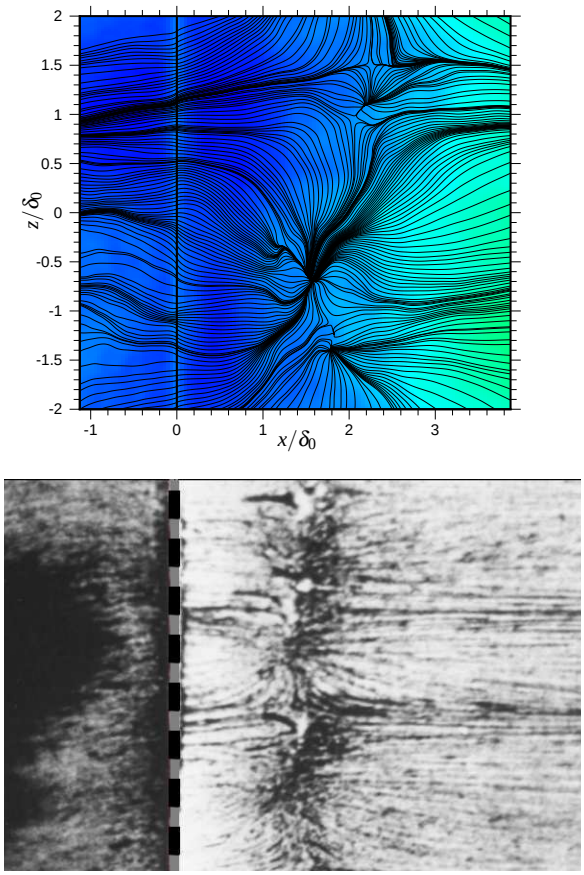

Figure 10. Comparison between oil-flow visualization from experiment and numerical surface skin friction pattern.

corresponding to experimental conditions is achieved, allowing for direct comparison. The results are validated successfully against the reference experiment. In particular a good agreement was achieved for surface-pressure and skin-friction distributions, mean velocity profiles, density and velocity fluctuations distributions. The combined effect of perturbations sequentially imposed on the turbulent boundary layer is investigated. It is shown that the expansion fan near the decompression corner destroys shocklets and streamwise vortices, while the level of turbulent fluctuation in the outer flow is high. The simulation provides a reliable database for further investigations.

Acknowledgments

This research was founded by the German Research Council (DFG) through the SFB TRR 40 project. Computing time was granted by the German National Supercomputing Center in Munich (LRZ).

REFERENCES

Adams, N.A., 2000, ”Direct simulation of the turbulent boundary layer along a compression ramp at M = 3 and Re = 1685,” J. Fluid Mech., vol. 420, 47–83.

Hickel, S. and Larsson, J., 2008, ”An adaptive local deconvolution model for compressible turbulence,” CTR, Proceedings of the Summer Program 2008.

Loginov, M. and Adams, N.A., 2006, ”Large-Eddy Simulation of Shock-Wave/Turbulent Boundary Layer Interaction,” J. Fluid Mech., vol. 565, 133–169.

Touber, E. and Sandham, N., 2009, ”Large-eddy simulation of low-frequency unsteadiness in a turbulent shock-induced separation bubble,” Theoret. Comput. Fluid Dynamics, vol. 23, 79–107.

Wu, M. and Martin, M.P., 2007, ”Direct numerical simulation of shockwave and turbulent boundary layer interaction induced by a compression Ramp,” AIAA Journal, vol. 45, 879–889.

Zheltovodov, A. A. and Yakovlev, V. N., 1986, ”Stages of developement, flowfield structure and turbulence characteristics of compressible separated flows in the vicinity of 2-D obstacles,” Preprint 2786 ITAM, USSR Academy of Sciences, Siberian Branch, Novosibirsk, (in Russian).

Zheltovodov, A.A., Trofimov, V.M., Schülein, E. and Yakovlev, V.N., 1990, ”An experimental documentation of supersonic turbulent flows in the vicinity of forward- and backward-facing ramps,” Tech. Rep. 2030, Institute of Theoretical and Applied Mechanics, USSR Academy of Sciences, Novosibirsk.